Journal of Power Sources 195 (2010) 4796–4803

Contents lists available at ScienceDirect

Journal of Power Sources

journal homepage: www.elsevier.com/locate/jpowsour

Fabrication and characterization of micro PEM fuel cells using pyrolyzed carbon current collector plates

Yun Wang[a,*], Liem Pham[a], Guilherme Porto Salerno de Vasconcellos[a,1], Marc Madou[b]

[a] Renewable Energy Resources Lab (RERL) and National Fuel Cell Research Center, Department of Mechanical and Aerospace Engineering, The University of California, 4231 Engineering Gateway, Irvine, Irvine, CA 92697-3975, USA
[b] Department of Mechanical and Aerospace Engineering, The University of California, Irvine, Irvine, CA 92697-3975, USA

ARTICLE INFO

Article history:
Received 28 January 2010
Received in revised form 17 February 2010
Accepted 18 February 2010
Available online 24 February 2010

Keywords:
Polymer electrolyte fuel cell
μPEMFC
Carbon
Bipolar plate
Pyrolysis

ABSTRACT

A novel fabrication technique for micro proton exchange membrane fuel cells (μPEMFCs) based on carbon-MEMS (C-MEMS) was optimized to yield higher performance cells. Polymer manufacturing is relatively easy compared to directly patterning graphite as is typically done to make fuel cell bipolar plates. In a C-MEMS approach, fuel cell bipolar plates are fabricated by first patterning polymer Cirlex® sheets. By subsequently pyrolyzing the machined polymer sheets at high temperature in an inert atmosphere, carbon bipolar plates with intricate groove structures to distribute the reactants are obtained. Using an improved assembly technique such as polishing the carbonized plates to minimize the contact resistance between gas diffusion layers (GDL) and bipolar plates, better pyrolysis temperature control and a better end plate design, a μPEMFC with a 0.64 cm^2 active surface was fabricated using the newly developed bipolar plates. At 1 atm and 25 °C a maximum power density of ~76 mW cm^{-2} was obtained, and at 2 atm and 25 °C ~85 mW cm^{-2} was achieved. These data are comparable with data reported in the literature for μPEMFCs and are a dramatic improvement over earlier results reported for the same C-MEMS based fuel cell. Electrochemical Impedance Spectroscopy (EIS) and cyclic voltammetry were carried out to characterize steady-state and transient characteristics of the novel C-MEMS fuel cell.

1. Introduction

Fuel cells electrochemically convert chemical energy stored in fuels directly and efficiently to electricity and because of their high efficiency and low emissions they have become the focus of a wide variety of new energy developments [1–3]. Among the different types of fuel cells, the polymer electrolyte fuel cells (PEFCs), also called polymer electrolyte membrane (PEM) fuel cells, have captured most of the public and R&D attention especially for mobile and portable applications [4,5]. In addition to providing high power density, PEFCs work at low temperature, only produce water as byproduct and can be compactly assembled. These factors make them one of the premier candidates as the next generation power generator to compete with batteries.

In Fig. 1 we schematically show a single PEMFC. A typical PEMFC consists of the following components: bipolar plates with grooved flow channels, gas diffusion layers (GDL), and a proton-conductive membrane with electrocatalyst coated on both sides. The bipolar plates, usually graphite or metal plates, play the important roles of electrically connecting the adjacent cells while at the same time distributing the reactant gases over the anode and cathode. Carbon-based substrates such as carbon paper and cloth constitute a typical GDL. The GDLs are placed on the membrane electrode assembly (MEA) and perform several functions: gas species transport, heat transport and last but not least the electrical connection between the bipolar plates and the catalyst layers on the proton-conductive membrane. The catalyst layers comprise the C/Pt or Pt alloy catalyst itself, an ionomer, and void space. The electrochemical reactions take place at the triple-phase boundary (TPB) of the catalyst layer, the gas phase and the ionically conductive membrane. The membrane, typically made of Nafion®, fulfills a dual role, i.e. as the gas/electron separator and for conducting protons. The Nafion® membrane is characterized by hydrophobic, fluorinated main chains with hydrophilic sulfonic acid pendant groups, allowing for protons to weakly interact with SO_3^- groups and to travel through the hydrated regions associated with those sulfonic groups.

Different from the traditional power generation in heat engines, fuel cells are electrochemical devices and their efficiency is not limited by the Carnot heat cycle. Efficiencies of more than 50% have been achieved in many commercial units operating at low currents. Fuel cell efficiency is especially high at smaller scales and in this regard, fuel cells may be ideal for powering portable/micro electrical devices and may have the potential to replace batteries whose

* Corresponding author. Tel.: +1 949 824 6004; fax: +1 949 824 8585.
E-mail address: yunw@uci.edu (Y. Wang).
[1] An exchange student from Brazil working at RERL of the UC Irvine.

0378-7753/$ – see front matter © 2010 Elsevier B.V. All rights reserved.
doi:10.1016/j.jpowsour.2010.02.050

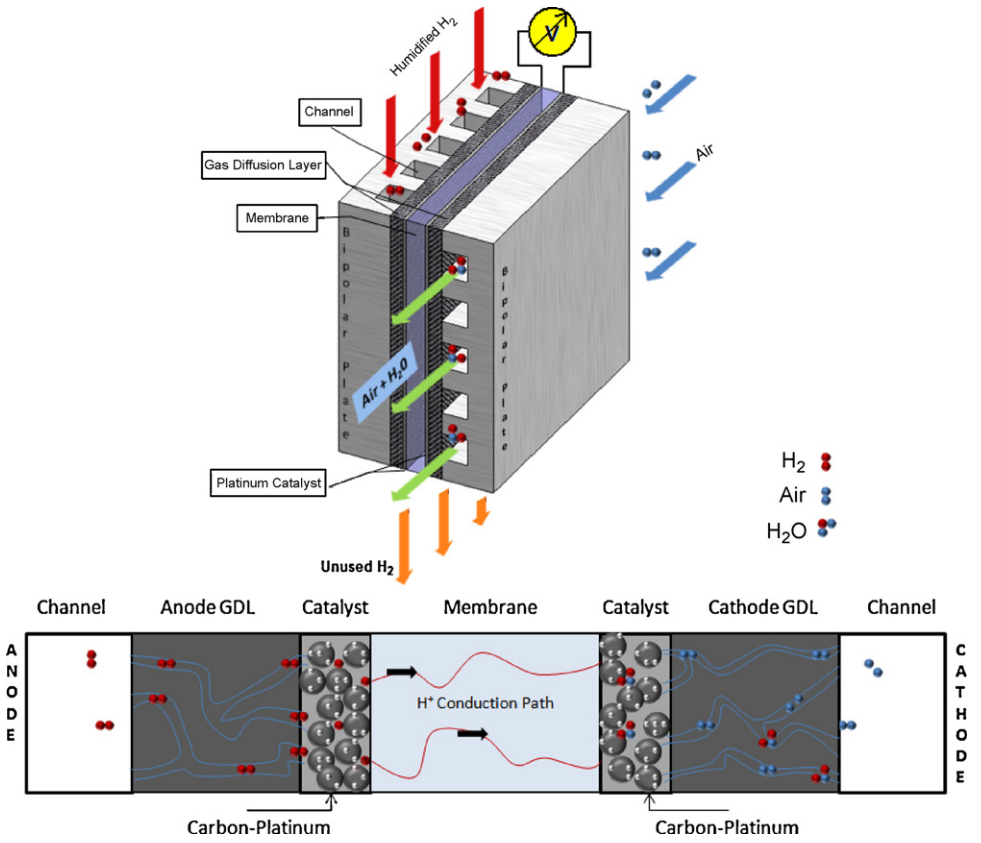

Fig. 1. The schematic of a PEFC. The MPL (micro porous layer) is shown as part of in the GDL in this figure.

energy capability is limited by the amount of chemicals stored. Due to their relative simple structure, PEMFCs can be developed at various sizes for different levels of power supply. The current technology also offers materials and manufacturing methods that afford the development of micro fuel cells, e.g. the Nafion membrane can now be fabricated as thin as ~18 μm; the catalyst layer may be as thin as ~7.5 μm and the GDL can be made at ~100 μm thick. The component that takes up most of the volume in a PEMFC is the bipolar plate. In addition to exhibiting the desired thermal/electrical conductivity, a bipolar plate material must also be suitable for cost-effective mass production, be resistant to corrosion, and be mechanically robust. Currently graphite composites are the most common material used for the bipolar plates [6]. One important issue with graphite bipolar plates is their intrinsic brittleness making it costly to machine. Other candidates for the bipolar plate material are metals [7–9]; their manufacturability and excellent thermal/electrical conductivity present major advantages over graphite. However, metals are typically susceptible to electrochemical/chemical corrosion. In addition to metals and graphite, silicon is frequently used in fabricating micro fuel cells due to the availability of a vast amount of silicon patterning techniques [10–14].

Several approaches have been proposed for micro fuel cell fabrication. Some authors suggest the possibility of membraneless micro fuel cells [15–18] by utilizing the low-Reynolds laminar flows typical in microflows circumventing the need of membranes to separate the anode and cathode gas streams. Hayase et al. [19] presented a fabrication technique to pattern the reactant channels and GDL in the Si wafer. Lee et al. [9] employed the LIGA [LIGA is the German acronym for X-ray lithography-technique (X-ray Lithographie), electro-deposition (Galvanoformung), and molding (Abformtechnik)] to fabricate flow fields in metallic bipolar plates. Ito et al. [10] utilized a technique similar to that used for machining of compact disks to create microgrooves in metal plates. Hahn et al. [20] used reactive ion etching (RIE) to machine microchannels in stainless steel plates. Hsieh et al. [21] proposed a SU-8 photoresist microfabrication process for the fuel cell flow structures. Cha et al. [22] employed various micro/nanofabrication processes, such as lithography, physical vapor deposition (PVD), and focused ion beam (FIB) etch/deposition, to fabricate flow field plates. Madou and co-workers [23,24] used carbon obtained by pyrolyzing polymer precursors (the so-called C-MEMS process) for the bipolar fluidic plates. They assembled both a single fuel cell and a three-cell stack. Their preliminary designs however indicated an extremely low performance.

In this paper, the C-MEMS method is employed to fabricate current collector bipolar plates with the aim to develop and optimize micro PEMFCs that are able to exhibit much higher performances than those reported earlier [23,24]. The bipolar microgrooves are prefabricated in Cirlex® as the polymer precursor material. Patterning of polymer sheets can be readily achieved by techniques such as molding and milling and in the case of photosensitive polymers even through lithography. Using the C-MEMS process the patterned polymer is then converted into grooved carbon plates at high temperature in an inert atmosphere. Studying the earlier published designs that failed to obtain a high fuel cell performance [23,24] we speculate now that the low performance might have been due to any of the following causes: (1) the extremely high Ohmic resistance as evidenced from the EIS results (see Fig. 14 in Ref. [24]); (2) leakage of fuel or oxidizer at the inlets; (3) shortcuts of the reactant flow in the serpentine gas channels. Causes 1 and 3 are closely linked to the details of the pyrolysis method, i.e. the Cirlex® surface can become warped during the carbonization process due to non-uniform heating. In the present design, we controlled the heating of the plates much better and polished the carbonized plates to minimize contact resistance between the GDLs and the bipolar plates (avoiding possible cause 1). This also avoids

the possible short-cuts of reactant flows in the serpentine gas channels due to uneven surfaces (avoiding cause 3). To avoid reactant leakage, we also improved the design of the inlet ports. Previously, to prevent leakage we used syringe needles glued to the end plates. However, the glue seals may not always be reliable and may break upon connection of the syringes to the gas supply hoses. To provide more reliable inlet/outlet ports, greater care was taken to design end plates that better integrate the key fuel cell components so as to avoid cause 2. Nafion 112 and carbon cloth were chosen as the electrolyte membrane and GDL, respectively. Both steady-state and transient fuel cell operations were characterized experimentally.

2. Material, fabrication and experimental

2.1. Material selection and fuel cell fabrication

The micro fuel cell we fabricated has an active surface area of 0.64 cm^2 with an overall thickness of ~3 mm. In addition to the components shown in Fig. 1, two end plates were designed/fabricated to assemble the fuel cell components.

2.1.1. Bipolar plates

Bipolar plates play the dual role of distributing the gaseous reactants via distribution channels carved into their surface and conducting electrons via the bulk of the solid plates. In order to uniformly supply reactants and avoid local reactant starvation, several flow fields have been investigated: typical designs include parallel, serpentine, pin type, and interdigitated flow fields [25–29]. Co- and counter-flow configurations may be adopted to feed the anode and cathode gas streams. The counter-flow configuration yields superior water management capabilities due to the internal humidification process it promotes. Channel dimensions profoundly affect fuel cell performance. Wang's analysis suggests that gas channel size impacts heat removal, Ohmic voltage loss and pumping capacity for the reactant streams [29]. In the current study, we choose the counter-flow configuration and a standard cross-section and spacing for the microgrooves. The bipolar plates are fabricated through high-temperature pyrolysis of polymer sheets, i.e. Cirlex® (a DuPont product) (dimensions: Cirlex 10 mm × 10 mm × 2 mm), see Fig. 2. The flow fields in these plates were first designed using Solidworks a 3D CAD software. These designs were then used as the input to FeatureCam software that is used to generate the G-code (the numerical control programming language) for a high-resolution CNC milling machine (resolution 0.0001 in.). As a typical design we did choose a simple serpentine configuration. The grooves in this design featured three U turns with an overall flow path length of ~3 cm. The cross-sectional dimension of the square shaped grooves was ~1.0 mm × 1.0 mm. The machined polymer plates were then transferred to a furnace with an inert environment for pyrolysis. The furnace temperature was ramped from room temperature to 300 °C in about 12 min. The heating unit is then turned off for 30 min to allow for a full cure and to thermally anneal the polyimide plates. After the 30 pause in heating ramp-up, the furnace temperature is increased to 900 °C in 60 min and is then kept at 900 °C for another 60 min for full conversion of the bipolar plates to carbon. Compared with previous work on C-MEMS fuel cells [23,24], we have optimized the detailed temperature control of the Cirlex® plates during the pyrolysis process. The resulting pyrolyzed plates feature a superior surface smoothness. To enhance surface smoothness even further, the pyrolyzed Cirlex® plates were also polished. In Fig. 3 we compare the machined raw Cirlex® plates with the pyrolyzed ones. The pyrolyzed plates have shrunk from the original dimensions by ~20%. Accordingly, the resulting carbon channels are smaller than the ones in the original Cirlex® sheets. Details regarding the C-MEMS process can be found in Ref. [23].

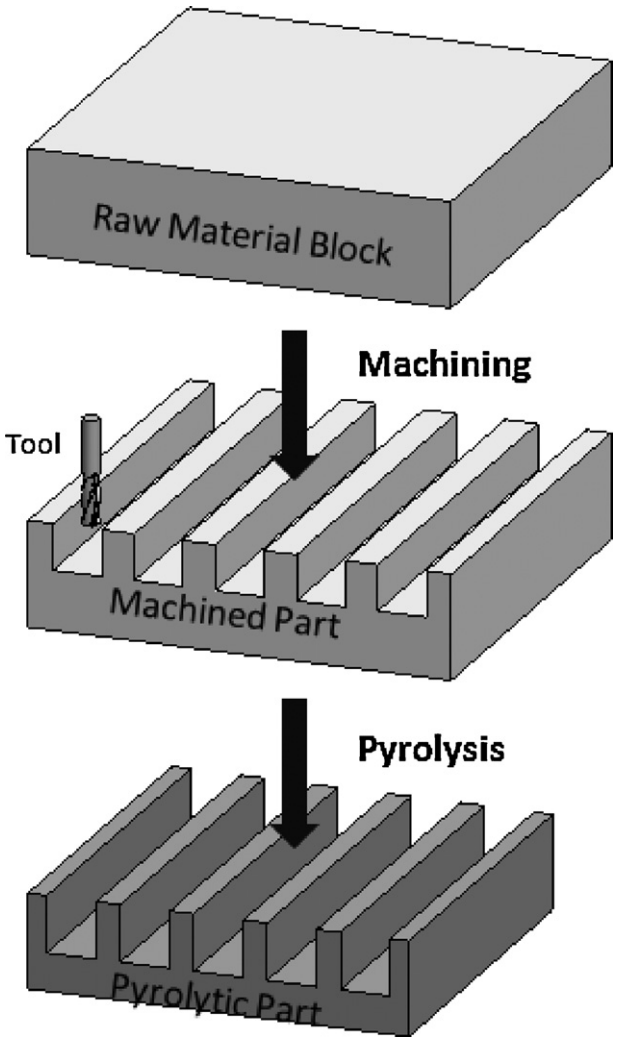

Fig. 2. The fabrication process of the carbon bipolar plates.

2.1.2. End plates

In order to assemble the different fuel cell components, end plates were designed and fabricated using plastics and metals so as to provide a mechanical support structure and to provide for reactant inlet/outlet ports. In the C-MEMS micro fuel cell, the bipolar plates are thin and brittle, making it almost impossible to directly mount fittings for feeding the gaseous reactants. For example, since carbon is so brittle it is difficult to machine threads directly into the bipolar plates. A novel design for the fuel cell end plates is shown in Fig. 4. The housing parts for the micro fuel cell feature a machined channel to accommodate an O-ring to seal the fuel cell in the center. A hole on each corner allows for alignment and bolting purposes, and two additional holes for reactant gases are created on each side of the square fuel cell chamber and to accommodate the inlet/outlet fittings. Note that this design makes for more reliable inlet/outlet ports for the fuel cell compared with the needles plus glue sealing method used in Refs. [23,24], and reduces the possibility of leakage during operation. Finally a small hole is drilled in the side wall of the endplates to fit a thermocouple for temperature measurements.

2.1.3. GDLs/MPL (micro porous layer)s

GDL/MPLs are important fuel cell components that electrically and thermally connect the bipolar plates and catalyst layers. In addition, GDLs/MPLs provide channels for the electrochemical reaction products. Preferred GDL/MPL materials must therefore

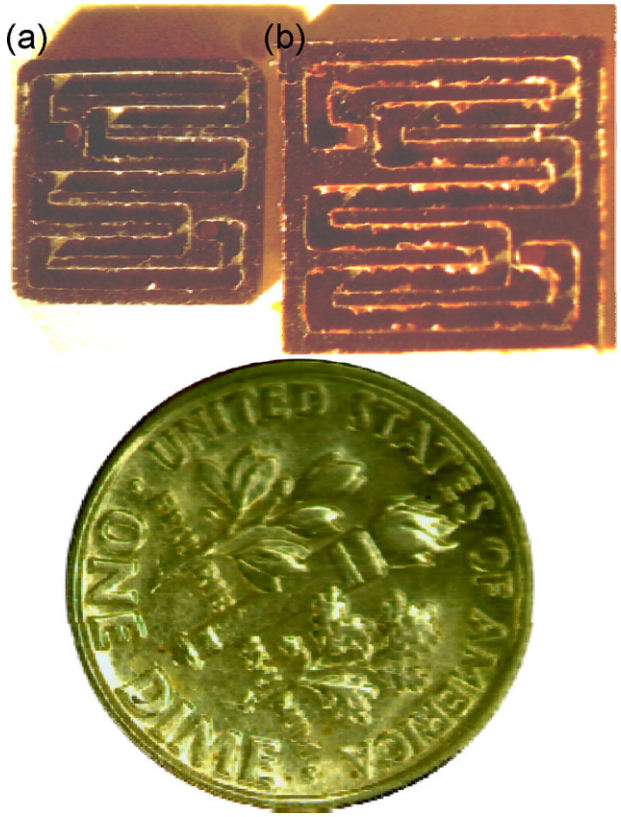

Fig. 3. Bipolar plate with a serpentine flow field: (a) after carbonization; (b) before carbonization.

exhibit high electrical/thermal conductivity and sufficient porosity. The GDL/MPL is usually treated hydrophobic by adding PTFE (polytetrafluoroethylene) to improve liquid water removal capacity. Typical GDL materials are carbon-fiber-based porous media such as carbon paper and cloth as shown in Fig. 5 where we show microscope pictures of carbon paper and carbon cloth. The carbon paper is non-woven and the fibers are bonded together by binders, the carbon cloth is a woven fabric, thus no binder is needed [30]. In both porous materials the carbon fibers constitute the primary path for electron and heat transfer but the two exhibit distinct performance differences in fuel cell operation due to their micro structure difference [31–34]. The carbon cloth shows a better performance at high humidity due to its rougher surface which alleviates liquid water coverage on the GDL surface [34]. In this work, we used a carbon cloth for the GDL with a PTFE content of ~15%.

2.1.4. MEA

The MEA is the "engine" of a fuel cell, it is the site where the electrochemical reactions take place. The MEA consists of catalyst layers coated on either side of a Nafion membrane. Pt-based materials are still the best choice for electrocatalysts in a PEM fuel cell. A Pt loading of ~0.4 mg cm^{-2} is typical in demonstration models and a lower ~0.1 mg cm^{-2} loading was reported in several studies at the experimental level [35–37]. To fabricate the MEA a polymer ionomer solution (Nafion, water and alcohol mixture) and carbon/Pt are mixed to form the catalyst ink, which is then coated uniformly on the GDL and dried to form an electrode layer. The thickness of a typical catalyst layer is ~10 μm. Despite this electrode thickness, the cathode reaction, the ORR (oxygen reduction reaction), is sluggish comparing with the anode HOR (hydrogen oxidation reaction), therefore a spatial variation of the reaction may occur across the catalyst layer [38]. Multilayer configurations can improve the electrode performance and catalyst utilization by optimizing the spatial distribution of the material composition [39–41]. In this study, we used a single layer electrode configuration. A Nafion membrane consists of a hydrophobic backbone and sulfonic acid hydrophilic pendant groups. Water and protons are able to transport through this membrane readily but the same membrane constitutes a high electrical resistance preventing a circuit shortcut. Water is essential for the ionic conductivity of the Nafion membrane and the dryer a membrane the higher its Ohmic resistance is. Water transport in the Nafion membrane plays a crucial role for fuel cell water management: electro-osmosis drives water from the anode to the cathode, while back-transport by diffusion or hydraulic permeation brings water back to the anode. The membrane thickness can affect the

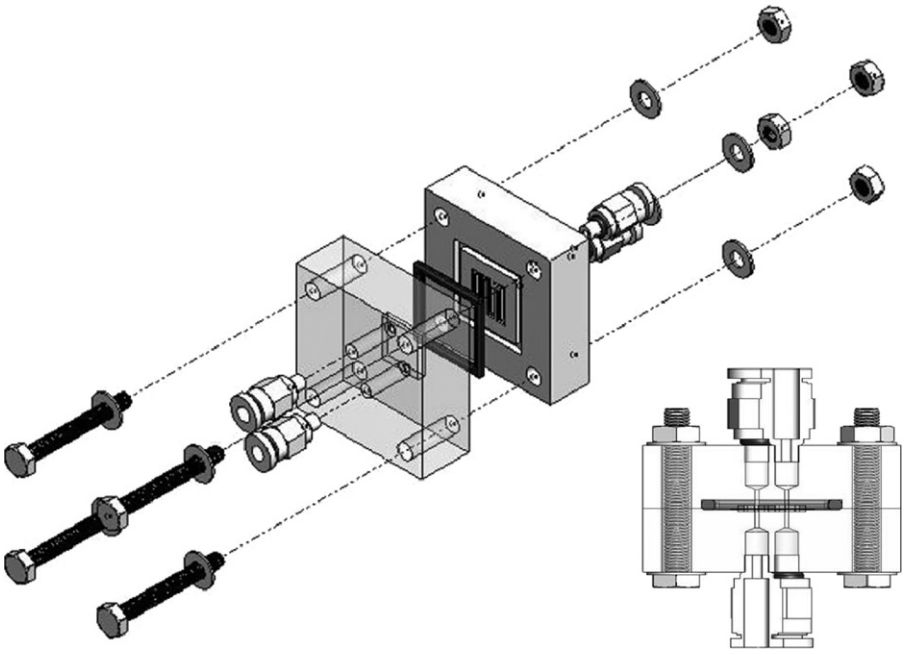

Fig. 4. Design of the end plates and fuel cell.

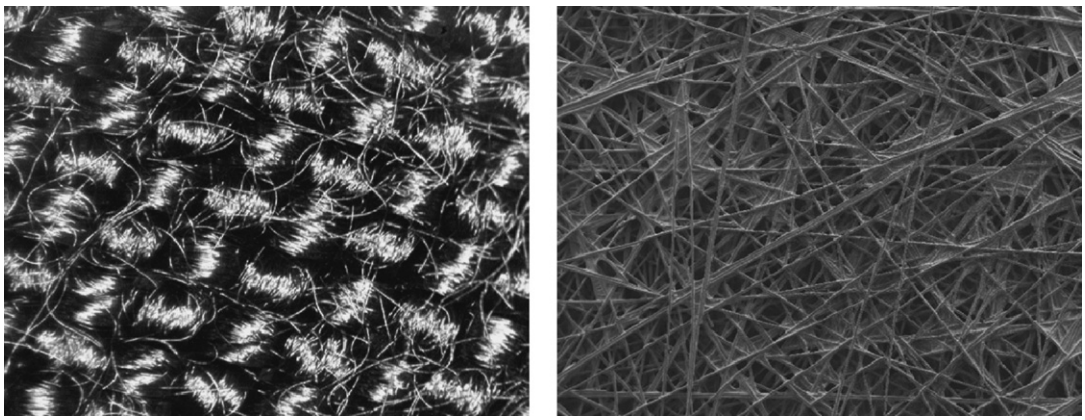

Fig. 5. Carbon cloth (left) and paper (right).

water back-transport as well as the proton conductance. A thicker membrane may be a better choice from a mechanical strength point of view, but it will increase the proton/water transport resistance and hence the Ohmic voltage loss. In this study, we choose N112 membrane. In Fig. 6 we show the MEA and GDL used in our experiments.

2.2. Experimental

In our experiments, the assembled micro PEM fuel cell (see Fig. 7) is connected to a fuel cell test system (see Fig. 8) via hoses and fittings. The fuel cell testing facilities include an E-load (electronic load), anode/cathode gas supply mass flow controllers (M100B Mass-Flo®), pressure sensors (to monitor the back pressures, and differential pressure between inlet and outlet), three temperature sensors (to monitor the inlet steams and fuel cell temperatures), bubbler temperature controllers (to control the humidification of reactant inlet flows), fuel cell temperature control unit with a heater, and frequency response analyzer. Manual back pressure units are installed to control the fuel cell pressure. Signals from the differential and absolute pressure sensors are acquired by the NI (national instrument) equipment. A thermocouple is inserted into the side wall of an end plate to monitor the fuel cell temperature.

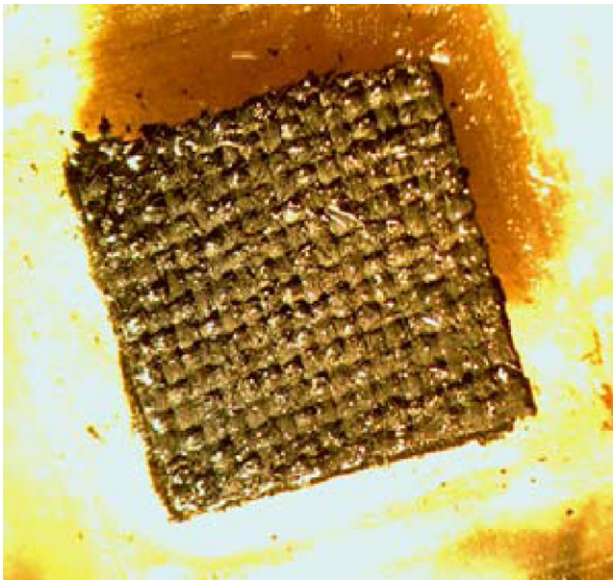

Fig. 6. Membrane electrode assembly (MEA) covered by carbon cloth gas diffusion layer (GDL) used in the fuel cell.

The Electrochemical Impedance Spectroscopy (EIS) tests were performed to investigate the internal Ohmic and reaction resistances. In addition, standard potential sweeping tests were conducted to investigate the dynamic operation of the fuel cell.

3. Results and discussion

For all experimental results presented below, the operating temperature was 25 °C and both sides of the fuel cell were kept fully humidified (Table 1). Room temperature operation is often possible for portable or micro electrical applications of fuel cells; because of the large surface/volume ratio for micro fuel cell systems, heat convection at the outer surface is indeed often sufficient to remove the waste heat. To simplify the control over the fuel cell, anode and cathode compartment gas flow rates of 20 and 50 sccm, respectively, were employed. In Fig. 9 we show the steady-state current–voltage and the power output for the current PEM fuel cell at three different pressures. The results show that the current micro fuel cell is able to produce up to 85 mW cm^{-2} at 25 °C at 2 atm. The higher the pressure, the better the cell performance with the difference between different pressures becoming more evident at higher current densities. This is primarily due to fact that the larger oxygen content at the higher pressures alleviates the mass transport polarization. Note that due to the low operating temperature the water saturation pressure is low and therefore water that is produced in the fuel cell reaction is likely to condense, leading to two-phase (liquid water-gas) flow. The water that is forming limits gaseous transport, thus reducing the limiting current. Importantly, despite this limitation, the power output of the current C-MEMS fuel cell is about two-order-of-magnitude higher than in previously efforts [23] and is now comparable with the maximum power densities achieved in most studies reported in the literature [42], e.g. ~82 mW cm^{-2} [43], 50 mW cm^{-2} [44], 30 mW cm^{-2} [21,45], 42 mW cm^{-2} [46] and 40–110 mW cm^{-2} [10].

In Fig. 10 we display the EIS testing results at three different pressures. The frequency range we covered was from 0.1 Hz to

Table 1
Geometrical and operating parameters.

Quantity	Value
Gas channel depth/width	0.5/0.8 mm
Active area	0.64 cm^2
Membrane	Nafion 112
Bipolar plate thickness	1.6 mm
Fuel cell dimension	1.0 mm × 1.0 mm
Fuel cell temperature, T	25 °C
Fuel cell operating pressure	1–2 atm
Anode/cathode humidification	100/100%

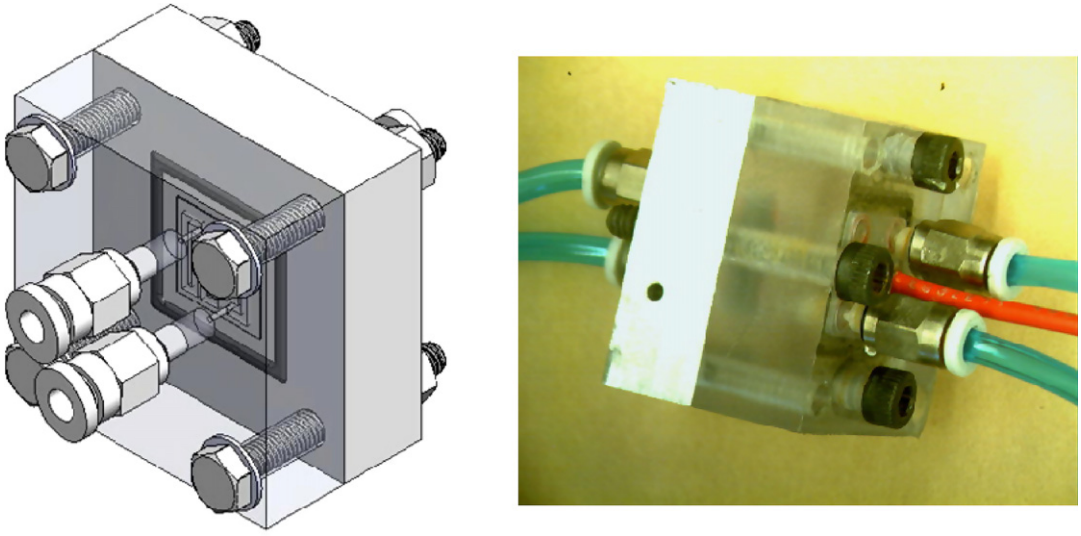

Fig. 7. Assembled micro PEM fuel cell: schematic (left); actual photo (right).

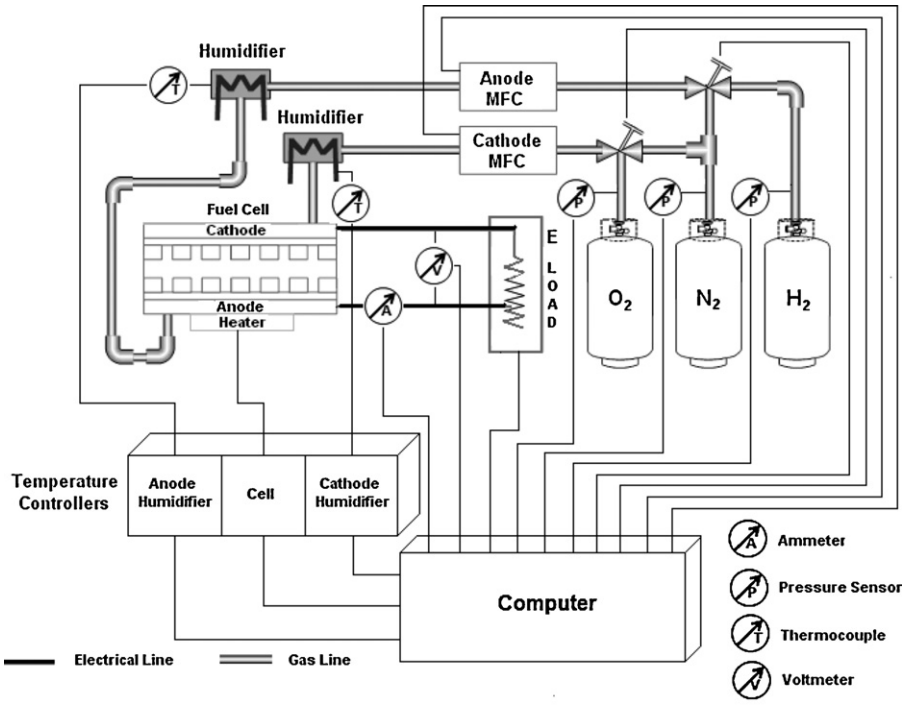

Fig. 8. Schematic of the fuel cell test facilities.

10^3 Hz. The results show that the series resistance is ~1.65 Ω, which is much smaller than our previous approach [24] and comparable with data reported by Ito et al. [10] and Hsieh et al. [21]. This measured series resistance includes the overall Ohmic resistance of the solid parts of the fuel cell and that of the electrolyte. In micro fuel cells, high resistances are often encountered due to the difficulty in controlling the contacts between their small-scale components, e.g. lack of sufficient compression between bipolar plates and GDLs. In our previous C-MEMS fuel cell efforts [24], a series resistance of over 100 Ω was found (more than 50 times the value of our current cell). This improved result was obtained by better surface control of the bipolar plates through better pyrolysis control and polishing of the C-MEMS structures, significantly reducing the Ohmic resistance in the fuel cell.

In Fig. 11 we show the results of potential sweep experiments at different sweep rates all at 1 atm. The forward voltage sweep test started at 0.9 and ended at 0.25 V. It can be seen that the cell dynamic performances are different at the different sweep rates. It is evident that the fastest sweep rate results in the lowest fuel cell performance. In addition, all dynamic performances are lower than the steady-state one illustrated in Fig. 9. A possible reason for the influence of sweep rate on performance is the dynamics of the water transport inside the fuel cell. There are two mechanisms of water transport in the membrane which greatly affect the water

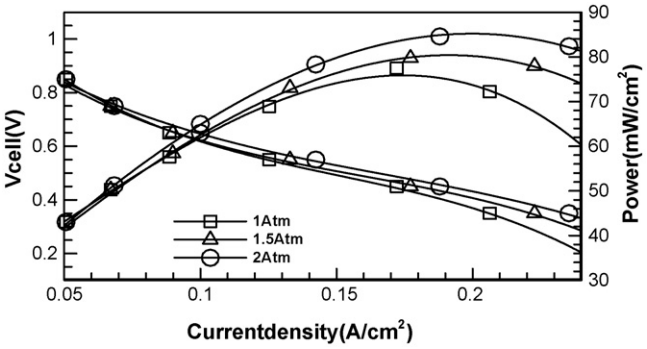

Fig. 9. Steady-state performance of the μPEMFC.

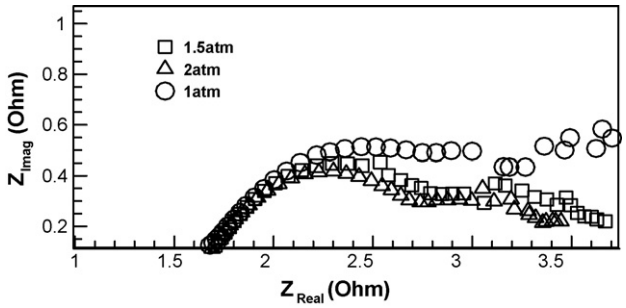

Fig. 10. Nyquist plot of the μPEMFC at three operating pressures all at 0.35 V (frequency: 0.1–1000 Hz).

management in the fuel cell: one is the water electro-osmotic drag that dehydrates the anode; the other is the back-transport by diffusion and hydraulic permeation that alleviates the anode dryness by delivering water from the cathode to anode. Though full humidification is applied to both sides of the membrane, the osmotic drag and low-temperature operation of the current cell can lead to severe anode dryness, particular for a thick membrane (N112). Water back-transport is due to the water diffusion in the membrane's hydrophilic regions and water hydraulic permeation driven by the pressure difference at the membrane surface arising from the capillary action. Both mechanisms are closely related to the cathode water content. Although the water production rate is proportional to the current density (Faraday's Law), the cathode water content increases nonlinearly with the current density partly due to the fact that liquid water transport in the cathode largely relies on capillary action that can be treated as a mechanism similar to

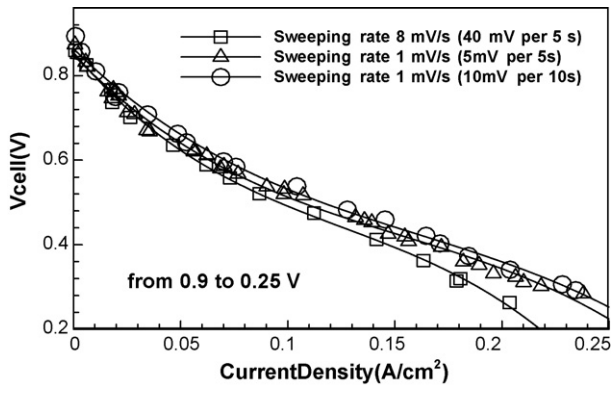

Fig. 11. Potential sweep tests at various voltage sweep rates all carried out at 1 atm.

"diffusion" with diffusivity as follow [38]:

$$D_c^{(l)} = -\frac{k_{rl}}{\nu^{(l)}}\sigma\ \cos(\theta_c)(K\varepsilon)^{1/2}\frac{dJ(s)}{ds} \quad (1)$$

where k_{rl} is the relative permeability for liquid, $\nu^{(l)}$ the liquid kinetic viscosity, σ the surface tension, K the permeability of the porous media, s the liquid saturation, ε the porosity of the porous media, and $J(s)$ the Leveret-J function. Note that Eq. (1) indicates the dependence of $D_c^{(l)}$ on the liquid saturation. Thus, at high current, the anode dryness may be greatly alleviated by the water back-transport due to the high water content at the cathode, therefore when sweeping from high voltage to low one (or from low current to high current density), the anode remains relatively drier: the faster the sweeping is, the drier the anode will be. A dry anode will increase the Ohmic polarization, reducing the cell performance. A detailed physical picture of water dynamic transport within the membrane is elucidated by Ref. [47] in their 3D numerical simulation.

In addition, the two cases at the same sweep rate of 1 mV s^{-1} but different step changes also exhibit an observable distinction in the I–V curve. The potential sweep test consists of many step changes in voltage. For the two cases at 1 mV s^{-1} rate, one applies 5 mV step change at the end of the period every 5 s; the other 10 mV at the end of the period every 10 s. The current density is recorded at the end of each voltage jump during sweep. It can be seen that the longer duration between two step changes (10 mV per 10 s) displays a slightly higher cell dynamic performance. This may also due to the water transport in the fuel cell: a large amount of water (=water flux × time duration) can transport back to the anode alleviating the anode dryness for the longer duration case.

4. Conclusions

In this paper, a micro PEMFC with a 0.64 cm^2 active area based on the C-MEM technique was designed, fabricated, and tested. We employed the pyrolysis method to fabricate the current collector plates by machining the flow channels in a polymer material and carbonizing the polymer in the high-temperature, inert environment. The end plates were designed to assemble the micro fuel cell and provide the necessary ports for reactant flow feeds. Both steady-state and dynamic performances of the fuel cell were tested. We achieved a fuel cell performance two-order-of-magnitude higher than our previous effort: maximum powers of ~0.85 mW cm^{-2} for 2 atm and 0.76 mW cm^{-2} for 1 atm at 25 °C are obtained, which are comparable to most data reported in the literature. We found that the dynamic performances at low temperature may be affected by the water transport in the membrane.

Acknowledgements

Partial support of this work by the Academic Senate Council on Research, Computing & Library Resources and UROP (Undergraduate Research Opportunities Program) at UCI is gratefully acknowledged.

References

[1] M.L. Perry, T.F. Fuller, J. Electrochem. Soc. 149 (2002) S59–S67.
[2] J. Larminie, A. Dicks, Fuel Cell Systems Explained, 2nd edition, John Wiley & Sons, 2003.
[3] C.Y. Wang, Chem. Rev. 104 (2004) 4727–4765.
[4] P. Costamagna, S. Srinivasan, J. Power Sources 102 (2001) 242–252.
[5] P. Costamagna, S. Srinivasan, J. Power Sources 102 (2001) 253–269.
[6] K. Roβberg, V. Trapp, Handbook of Fuel Cells—Fundamentals, Technology and Applications, John Wiley & Sons, Ltd., New York, 2003, pp. 308–314.
[7] J. Wind, A. LaCroix, S. Braeuninger, P. Hedrich, C. Heller, M. Schudy, Handbook of Fuel Cells—Fundamentals, Technology and Applications, John Wiley & Sons, Ltd., New York, 2003, pp. 295–307.

[8] J.P. Meyers, H.L. Maynard, J. Power Sources 109 (2002) 76–88.
[9] S.J. Lee, Y.P. Chen, C.H. Huang, J. Power Sources 145 (2005) 369–375.
[10] T. Ito, S. Kaneko, M. Kunimatsuz, Electrochem. Solid-State Lett. 12 (2009) B154–B157.
[11] T.J. Yen, N. Fang, X. Zhang, G.Q. Lu, C.Y. Wang, Appl. Phys. Lett. 83 (2003) 19.
[12] M. Hayase, T. Kawase, T. Hatsuzawa, Electrochem. Solid-State Lett. 7 (8) (2004) A231–A234.
[13] J.G.A. Brito-Neto, K. Kondo, M. Hayase, J. Electrochem. Soc. 155 (2008) D78–D82.
[14] D. Modroukas, V. Modi, L. Frechette, J. Micromech. Microeng. 15 (2005) S193–S201.
[15] J.L. Cohen, D.A. Westly, A. Pechenik, H.D. Abruna, J. Power Sources 139 (2005) 96–105.
[16] A. Bazylak, D. Sinton, N. Djilali, J. Power Sources 143 (2005) 57–66.
[17] Hasegawa, K. Shimotani, K. Kishi, H. Watanabe, Electrochem. Solid-State Lett. 8 (2005) A119–A121.
[18] E.R. Choban, P. Waszczuk, P.J. Kenis, Electrochem. Solid-State Lett. 8 (2005) A348–A352.
[19] M. Hayase, T. Kawase, T. Hatsuzawa, Electrochem. Solid State Lett. 7 (2004) A231.
[20] R. Hahn, S. Wagner, A. Schmitz, H. Reichl, J. Power Sources 131 (2004) 73–78.
[21] S.S. Hsieh, C.F. Huang, J.K. Kuo, H.H. Tsai, S.H. Yang, J. Solid State Electrochem. 9 (2005) 121–131.
[22] S.W. Cha, R. O'Hayre, Y. Saito, F.B. Prinz, J. Power Sources 134 (2004) 57–71.
[23] B.Y. Park, M.J. Madou, J. Power Sources 162 (2006) 369–379.
[24] P.-C. Lin, B.Y. Park, M.J. Madou, J. Power Sources 176 (2008) 207–214.
[25] D.P. Wilkison, O. Vanderleeden, in: W. Vielstich, H. Gasteiger, A. Lamm (Eds.), Handbook of Fuel Cells: Fundamentals, Technology and Applications, vol. 3, Ch. 27, John Wiley & Sons, Ltd., 2003.
[26] T.V. Nguyen, W. He, in: W. Vielstich, H. Gasteiger, A. Lamm (Eds.), Handbook of Fuel Cells: Fundamentals, Technology and Applications, vol. 3, Ch. 28, John Wiley & Sons, Ltd., 2003.
[27] X. Li, I. Sabir, Int. J. Hydrogen Energy 30 (4) (2005) 359–371.
[28] Y. Wang, S. Basu, C.-Y. Wang, Modeling two-phase flow in PEM fuel cell channels, J. Power Sources 179 (2008) 603–617.
[29] Y. Wang, J. Electrochem. Soc. 156 (10) (2009) B1124–B1133.
[30] M. Mathias, J. Roth, J. Fleming, W. Lehnert, in: W. Vielstich, H. Gasteiger, A. Lamm (Eds.), Handbook of Fuel Cells: Fundamentals, Technology and Applications, vol. 3, John Wiley & Sons, Ltd., 2003.
[31] T.R. Ralph, G.A. Hards, J.E. Keating, S.A. Campbell, D.P. Wilkinson, M. Davis, J. St-Pierre, M.C. Johnson, J. Electrochem. Soc. 144 (11) (1997) 3845.
[32] M.V. Williams, E. Begg, L. Bonville, H.R. Kunz, J.M. Fenton, J. Electrochem. Soc. 151 (2004) A1173.
[33] T. Frey, M. Linardi, Electrochim. Acta 50 (1) (2004) 99.
[34] Y. Wang, C.Y. Wang, K.S. Chen, Electrochim. Acta 52 (2007) 3965–3975.
[35] J. Zhang, PEM Fuel Cell Electrocatalysts and Catalyst Layers Fundamentals and Applications, Springer, 2008.
[36] H. Rabat, P. Brault, Fuel Cells 2 (2008) 81.
[37] L. Xiong, A. Manthiram, Electrochim. Acta 50 (2005) 3200.
[38] Y. Wang, Xuhui Feng, J. Electrochem. Soc. 155 (12) (2008) B1289–B1295.
[39] Y.-G. Yoon, T.-H. Yang, G.-G. Park, W.-Y. Lee, C.-S. Kim, J. Power Sources 118 (2003) 189–192.
[40] P.P. Mukherjee, C.Y. Wang, J. Electrochem. Soc. 154 (2007) B1121.
[41] Y. Wang, X. Feng, J. Electrochem. Soc. 156 (3) (2009) B403–B409.
[42] N.T. Nguyen, S.H. Chan, J. Micromech. Microeng. 16 (2006) R1.
[43] S.H. Chan, N.T. Nguyen, Z. Xia, Z.G. Wu, J. Micromech. Microeng. 15 (2005) 231.
[44] M.A. Müller, C. Müller, F. Gromball, M. Wöfle, W. Menz, Microsyst. Technol. 9 (2003) 159.
[45] J. Yeom, G.Z. Mozsgai, B.R. Flachsbart, E.R. Choban, A. Asthana, M.A. Shannon, P.J.A. Kenis, Sens. Actuators B 107 (2005) 882.
[46] A. Heinzel, C. Hebling, M. Müller, M. Zedda, C. Müller, J. Power Sources 105 (2002) 250.
[47] Y. Wang, C.Y. Wang, Electrochim. Acta 51 (2006) 3924–3933.